

Defect Morphology in Ti-6Al-4V Parts Fabricated by Selective Laser Melting and Electron Beam Melting

Haijun Gong*, Khalid Rafi*, N.V. Karthik *, Thomas Starr†, Brent Stucker*

*Department of Industrial Engineering, †Department of Chemical Engineering,
J. B. Speed School of Engineering, University of Louisville, Louisville, KY 40292

Accepted August 16th 2013

Abstract

In order to investigate the morphology of defects present in Selective Laser Melting (SLM) and Electron Beam Melting (EBM) processes, Ti-6Al-4V specimens were fabricated with varying porosity using non-optimum processing parameters. Defective specimens were sectioned and polished for microscopy. Image processing was adopted for statistically analyzing the characteristics of defects, such as distribution of defect area and dimensional proportion of each defect. It is found that defect morphology is influenced by process parameters as a result of a variation in the melt pool. Image processing of a cross-section could be a feasible way for calculating porosity of specimens.

1. Introduction

Selective Laser Melting (SLM) and Electron Beam Melting (EBM) are two common powder bed fusion processes within Additive Manufacturing (AM) for fabricating parts from metallic powders [1]. The SLM process selectively melts metallic powder using a focused laser beam. The melted powder attaches to the previous layer or support structure and solidifies in a short time. After that, a layer of new powder is recoated upon the current layer for the following layer melting [2]. At present, multiple materials can be utilized for SLM such as stainless steel, maraging steel, cobalt chromium and titanium alloys. The EBM process is similar. But, an electron beam, which is generated by a tungsten filament in the electron beam gun, is used instead of a laser beam. When the electrons penetrate the powder surface and further into the powder grains, their kinetic energy is converted into thermal energy [3]. Titanium Ti-6Al-4V and cobalt chromium powder are well developed for EBM.

Numerous studies on SLM and EBM have been carried out for process and material development. Additively manufactured materials were also tested and compared to that made from conventional methods. Due to their distinguished layer adding process and rapid cooling rate, SLM and EBM materials exhibit special microstructures and outstanding mechanical properties. Ti-6Al-4V powders are widely used in SLM and EBM processes for their inherent properties of fracture resistance, fatigue behavior, corrosion resistance and biocompatibility [4]. However, defects can be easily formed in additively manufactured Ti-6Al-4V material depending upon the influence of multiple factors. Thus, an investigation of defect morphology is helpful for understanding their effects on material properties.

AM powder bed fusion processes can be regarded as a type of Powder Metallurgy (PM) process [5], which are commonly used to produce porous parts. When an AM process is utilized to fabricate porous parts, it can be used to create structures which exhibit extreme flexibility in structural diversity and porosity characteristics if the morphology and distribution of defects in Ti-6Al-4V material is well-understood.

This paper studies the dimensional distribution, morphology of defects, and porosity generated by varying processing parameters in SLM and EBM. The reasons for defect formation are discussed. Variations in defect morphology with different energy input are analyzed. The statistical results are thus a good reference for future comparisons with traditional PM-produced porous materials.

2. Material and method

2.1 Powder Property

Raymor Ti-6Al-4V powder (Grade 23) with an apparent density of 2.55 g/cm^3 was used for SLM process. It has a particle size distribution between $17.36 \mu\text{m}$ (D_{10}) and $44.31 \mu\text{m}$ (D_{90}) with Mean Volume Diameter around $30 \mu\text{m}$. Lots of fine particles are included in Raymor Ti-6Al-4V powder. Arcam Titanium Ti-6Al-4V ELI powder was used for EBM process. Its apparent density is no more than 2.7 g/cm^3 . The particle size is normally distributed between $46.94 \mu\text{m}$ (D_{10}) and $99.17 \mu\text{m}$ (D_{90}) with a Mean Volume Diameter around $72.69 \mu\text{m}$. Both Raymor and Arcam powder particles are spherical.

2.2 Fabrication of Ti-6Al-4V Specimens

Porosity (R_D) of additively manufactured Ti-6Al-4V specimens can be estimated by measuring density using Archimedes method, and then compared with nominal density of Ti-6Al-4V material. Lower measured densities result in larger porosities.

A process window, as shown in Fig. 1, illustrates the effect of various laser power and scanning speeds when using SLM to process Raymor Ti-6Al-4V powder. Processing parameters can be divided into four melting zones. Zone I parameters result in nominally fully dense specimens. Specimens built at a high energy densities with Zone II parameters result in over melting. Defects are often generated in these specimens. Ti-6Al-4V powder is not completely melted using lower energy Zone III parameters, which results in pores and voids. Specimens cannot be successfully built using Zone OH parameters due to serious thermal deformations.

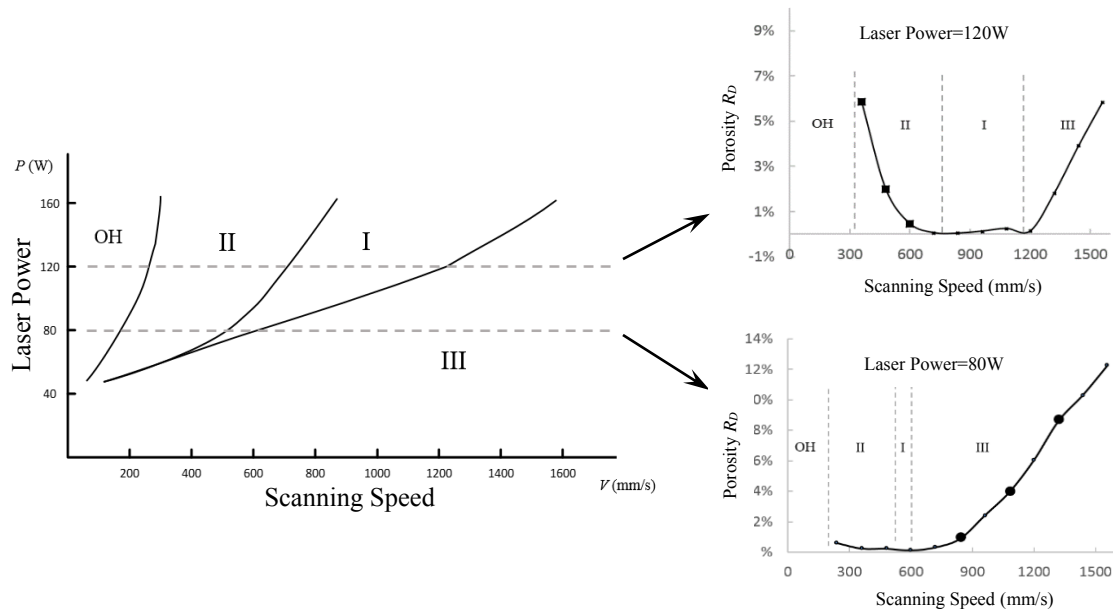


Fig. 1 Process Window of SLM and Porosity Distribution at 120W and 80W

In previous research, it was found that specimens can be built with various porosity distribution when using processing parameters, such as laser power and scanning speed, from different melting zones. Thus, investigations about defect morphology are primarily based on specimens when the laser power is equal to 80W and 120W, as shown in Fig. 1. Zone III processing parameters at elevated scanning speeds are of particular interest in this study because they are able to fabricate specimens with controlled porosity. An EOS M270 Direct Metal Laser Sintering (DMLS) system was utilized for building SLM specimens in this study.

An Arcam S400 EBM system was utilized in this study. Changes to beam current and scanning speed independently do not cause porosity in specimens, because the Arcam system dynamically coordinates these two parameters to achieve a steady melt pool size. However, “line offset” and “focus offset” can be varied to make porous specimens. Line offset refers to the distance between two hatch lines. And focus offset is the additional current running through the respective electromagnetic coil and can be translated into an offset of the focal plane from its zero position and thus a change in beam area [6]. Increased line offset results in lower energy densities, which forms voids in Ti-6Al-4V specimens. Increased focus offset increases beam diameter, thus lowering energy density and generating porosity.

Fig. 2 shows porosity distribution by varying line offset. It can be seen that the porosity value increases when the line offset value is increased, especially when the line offset is beyond 0.18mm. As shown in Fig. 3, apparent porosity (> 0.5%) appears when focus offset is larger than 16mA. Particularly at 20mA and 24mA, the increased focus offset causes a sharp increase in porosity in Ti-6Al-4V specimens. In order to investigate the defect characteristics, EBM specimens were built by increasing line offset and focus offset. In SLM and EBM processes, a number of processing parameters can be utilized to create specimens with a certain amounts of porosity, such as Zone II and III parameters of SLM or increased line offset and focus offset of EBM. These parameters are called “marginal parameters” in this study.

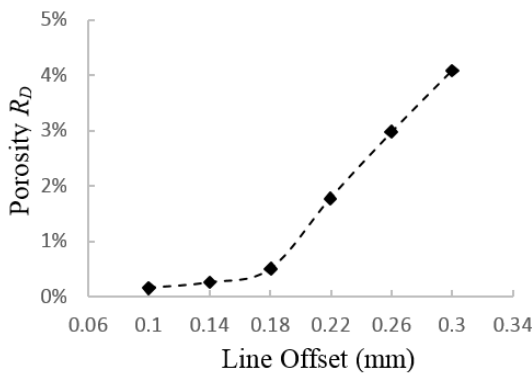


Fig.2 EBM Porosity versus Line Offset

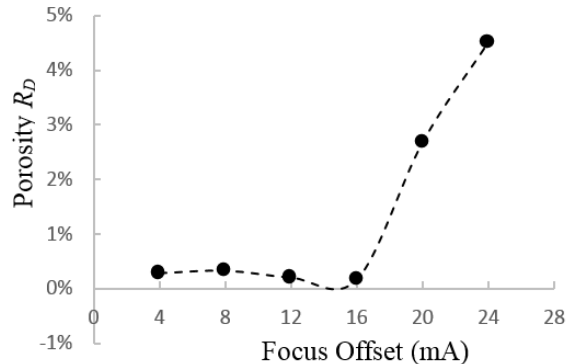


Fig.3 EBM Porosity versus Focus Offset

2.3 Image Processing Method

For each marginal parameter combination, two cubical Ti-6Al-4V specimens were sectioned and polished for microscopy. One specimen was cut along the horizontal plane; the other along vertical plane, as shown in Fig. 4. Cross sections were polished and then observed under optical microscope. Micrographs were taken for image processing process using Matlab R2012a.

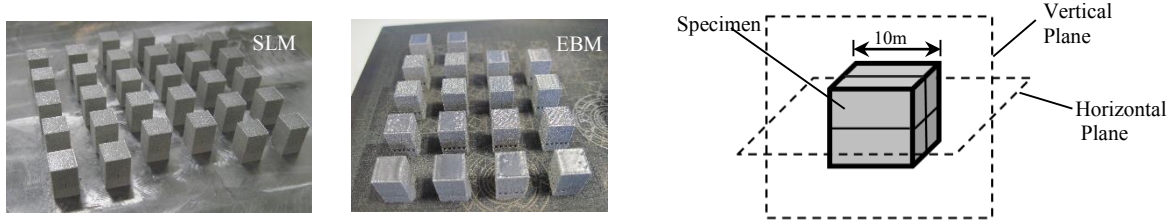


Fig. 4 Ti-6Al-4V Specimen

Micrographs were converted to binary images in order to highlight the features of the defective region. When a pixel's luminance of the original image is less than a user-selected threshold value, the pixel will be replaced with a value of 1 and other pixels will be replaced with a value of 0. In this paper, the threshold value is selected as 0.2. By doing this, the solid region is shown as a black color, while defective areas are white. Images which included contamination or polishing scratches were "cleaned" using a de-noising algorithm. For each defect, an area value could be obtained by counting pixels and then multiplying by individual pixel area. All defect areas can be summed up and then divided by cross sectional area to calculate image processing porosity (R_I). Certain descriptors such as circularity, convexity, and elongation are also employed for characterizing defect morphology in this study according to:

$$\text{Circularity} = 4\pi A / P^2 \quad (1)$$

$$\text{Convexity} = P_{\text{convexhull}} / P \quad (2)$$

$$\text{Elongation} = 1 - (L_{\text{minor}} / L_{\text{major}}) \quad (3)$$

where A is area, P is actual perimeter, $P_{\text{convexhull}}$ is the convex hull perimeter, L_{minor} is the minor axis length, and L_{major} is the major axis length. A perfect circle has a circularity of 1 while an irregular object has a circularity value closer to 0. Convexity is a measure of the surface roughness of a defect. A smooth shape has a convexity of 1 as the convex hull perimeter is exactly the same as the actual perimeter. A very irregular object has a convexity closer to 0 as the actual perimeter is greater than the convex hull perimeter due to the fine surface features. The major axis length of the defective area refers to the length of the major axis of the ellipse that has the same normalized second central moments as the region. Similarly, the minor axis length specifies the length of the minor axis. A shape symmetrical in all axes such as a circle or square will have an elongation value of 0 whereas shapes with large aspect ratios will have an elongation closer to 1.

3. Results and Discussion

Statistical distributions of the morphological descriptors of defects in each cross section are illustrated by histograms. Characteristics of defect morphology are analyzed and compared according to these distributions. Melt pool variation is discussed to explain defect formation.

3.1 Characterization of SLM Defects

3.1.1 Defect Morphology of Zone II Defects

When laser power, hatch spacing and layer thickness are constant, increasing the scanning speed will lower the energy density during SLM [2]. Fig. 5 shows horizontal and vertical cross sections of Ti-6Al-4V specimens built using Zone II marginal parameters, with scanning speed ranging from 360mm/s to 600mm/s.

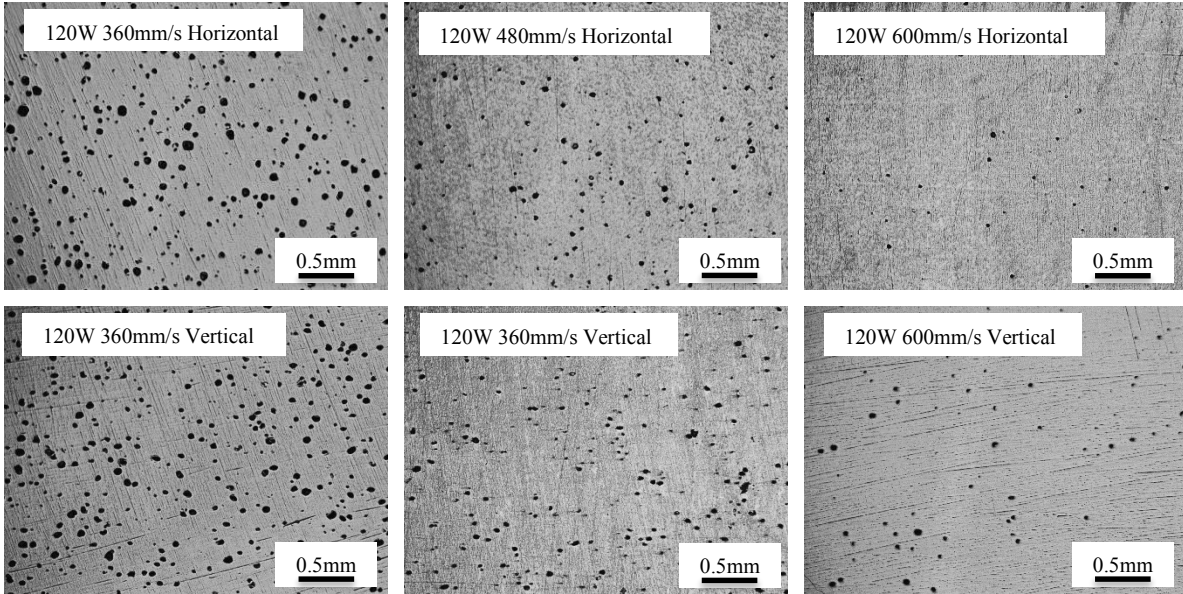


Fig. 5 Cross Section of SLM-produced Zone II Specimens

It can be seen that the defect amount decreases gradually when increasing the scanning speed to the fully dense melting zone. Defects are randomly spread on the horizontal and vertical cross sections. The defect dimension is also reduced with decreasing porosity. This trend is verified by the histograms in Fig. 6 (a) by the defects' area and their frequency of occurrence. Large defects only appears with higher porosity. Zone II defects are typically round in shape. Their morphology is well interpreted by the histograms of circularity, convexity, and elongation, as shown in Fig. 6 (b), (c) and (d).

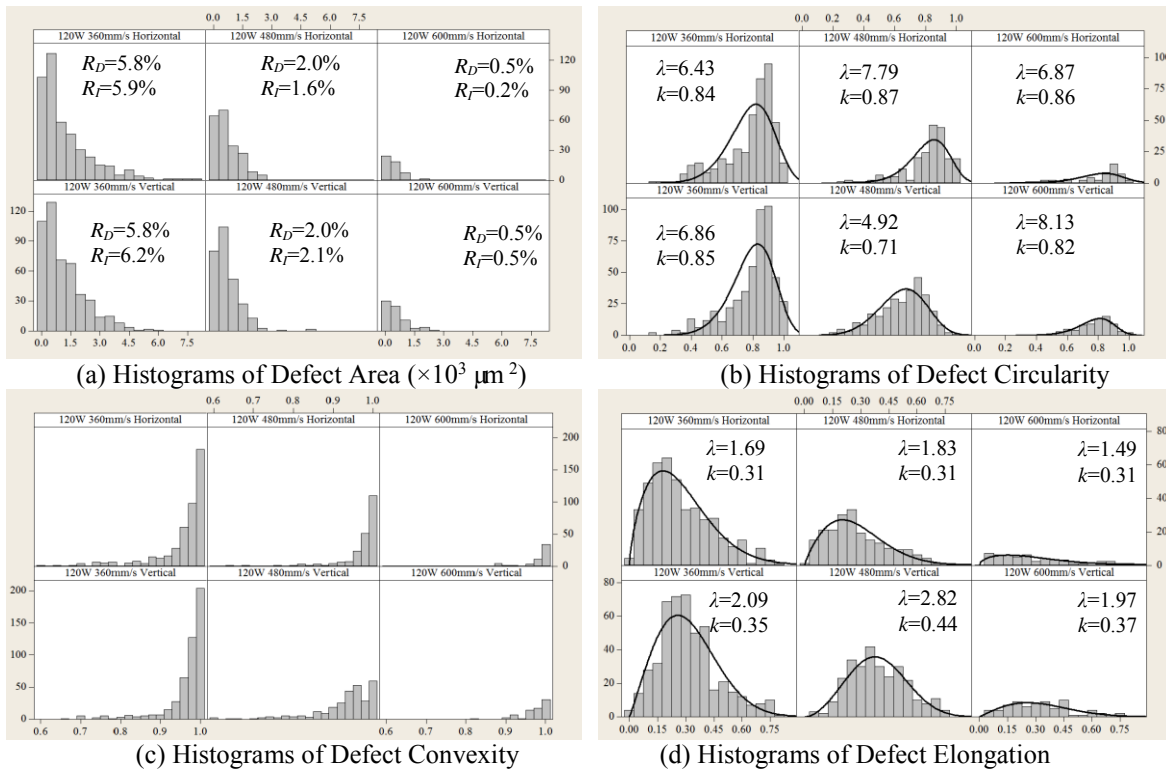


Fig. 6 Distribution of Defect Morphology of SLM-produced Zone II Specimen

As shown in Fig. 6 (b), a fitting curve shows a Weibull distribution with right skewness for defect circularity. Most Zone II defects have circularity values close to 1, which means they are circular or near-circular. Moreover, all Zone II defects have a convexity value larger than 0.5, as shown in Fig. 6 (c). A circular contour is a typical convex shape. Thus, it is easy to understand why most Zone II defects have a convexity value close to 1. As shown in Fig. 6 (d), the fitting curve of Zone II defect elongation also shows a Weibull distribution, but with different shape compared to circularity. Their left skewness indicates that the minor axis length is close to the major axis length, but not completely equal. According to the circularity and elongation distribution, it can be concluded that most defects have an elliptical contour for Zone II specimens. The shape parameter λ and scale parameter k of the Weibull fitting curve show slight difference between horizontal and vertical cross sections. This implies that the elliptical contours of Zone II defects are distinguishable based upon orientation and thus the material has porosity anisotropy. The λ value of Zone II defect elongation is closer to 0 in the horizontal direction than in the vertical direction. This demonstrates that defects are more circular in the plane parallel to scan surface.

3.1.2 Defect Morphology of Zone III Defects

Cross sections of Ti-6Al-4V specimens built by Zone III marginal parameters are shown in Fig. 7. Laser power is kept constant at 80W. Scanning speed ranges from 840mm/s to 1320mm/s. When the scanning speed is far away from Zone I, the energy density will be lowered which results in incomplete melting during the SLM process. It is noted that the porosity increased with increasing scanning speed.

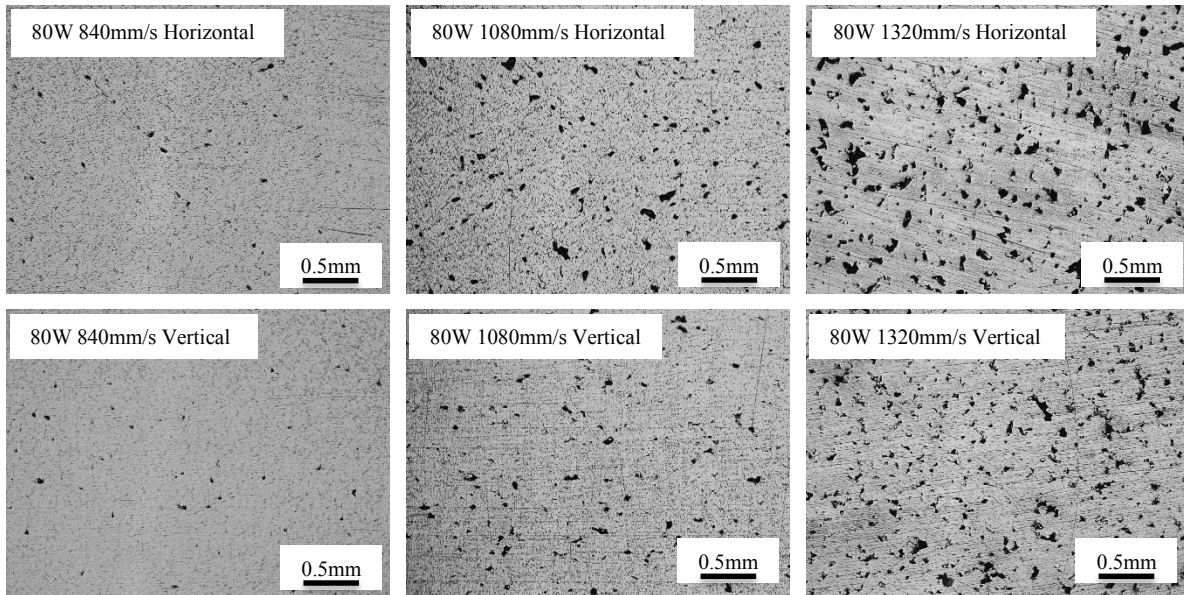


Fig. 7 Cross Section of SLM-produced Zone III Specimens

Defect dimension increases when increasing scanning speed. Similar to Zone II defects, the higher the porosity, the larger the defect dimension. However, unlike Zone II defects, Zone III defects are in irregular shape, in both horizontal and vertical cross sections. Large defects appears in Zone III specimens but with a small amount, as shown in Fig. 8 (a).

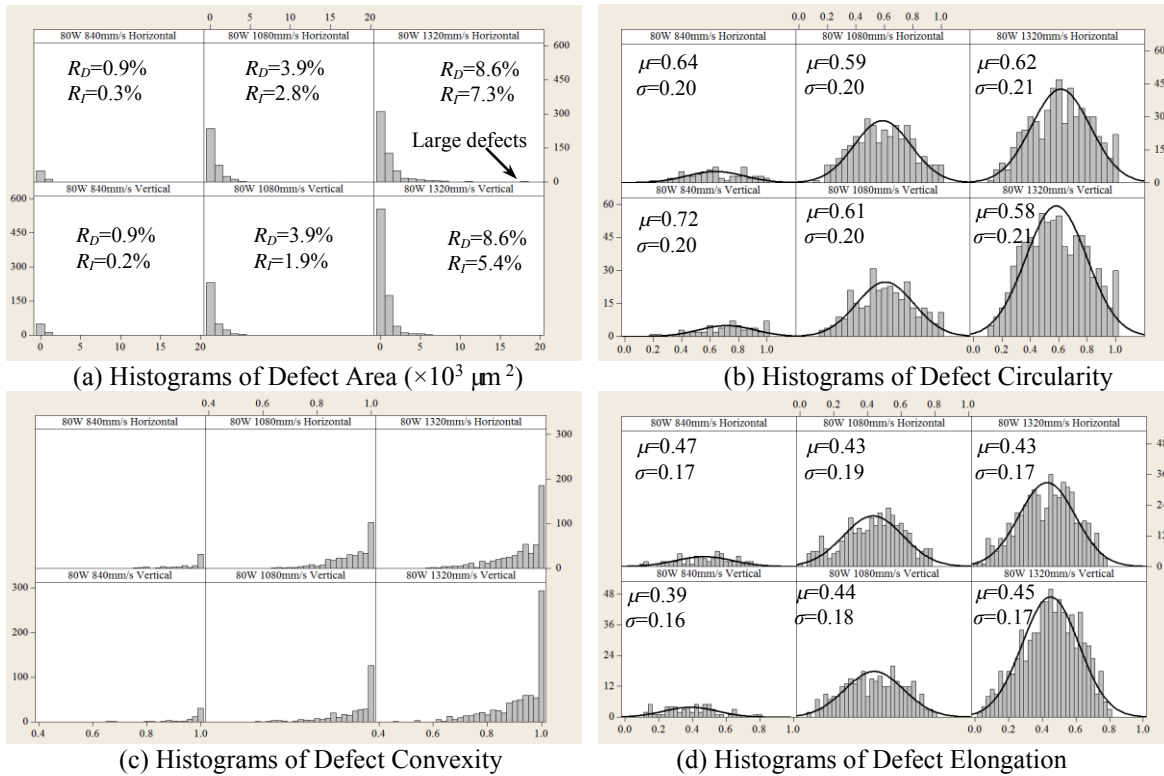


Fig. 8 Distribution of Defect Morphology of SLM-produced Zone III Specimen

The morphology of Zone III defects is different from Zone II defects, according to the distribution fitting curves of circularity and elongation. Fig. 8 (b) and (d) show that the circularity and elongation are all normally distributed, no matter whether in horizontal or vertical cross sections. Only a few Zone III defects are circular. Most of them are very irregular. The normal distributions of elongation have mean values ranging from 0.39 to 0.47, with standard deviation from 0.16 to 0.19. It can be seen that more than 70% of Zone III defects have an elongation value less than 0.5. Only 4% of Zone III defects have elongation value larger than 0.7, which means a long and narrow contour. As shown in Fig. 8 (c), some Zone III defects show concave characteristics, which illustrates their irregular shape.

3.1.3 Comparison of Defect Morphology in Zone II and Zone III Specimens

Generally, Zone II and Zone III defects show quite different morphological characteristics, especially in circularity and elongation. In order to further characterize the morphology, specimens with Zone II and Zone III defects are compared in Fig. 9. Both specimens have similar porosity ($\sim 5.8\%$). It is notable that the energy density of marginal parameters (120W&360mm/s) in Zone II is higher than that of Zone III marginal parameters (120W&1560mm/s).

Most Zone II defects are round in shape, while Zone III defects are large with an irregular shape. From Fig. 10 (a), it can be seen that most Zone II defects are have an area less than $6 \times 10^3 \mu\text{m}^2$, while some Zone III defects have areas up to $14 \times 10^3 \mu\text{m}^2$.

Weibull distribution is a proper choice to describe Zone II defect morphology, while Zone III defect morphology can be described using a normal distribution. The Weibull distribution statistically verifies that most Zone II defects are circular contour in both horizontal and vertical cross sections.

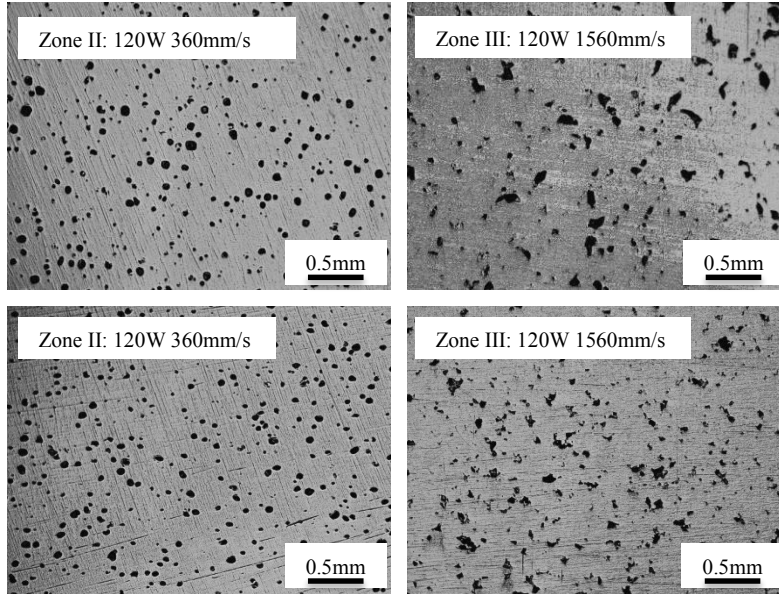


Fig. 9 Cross Section of SLM-produced Specimen (120W 360mm/s vs. 120W 1560mm/s)

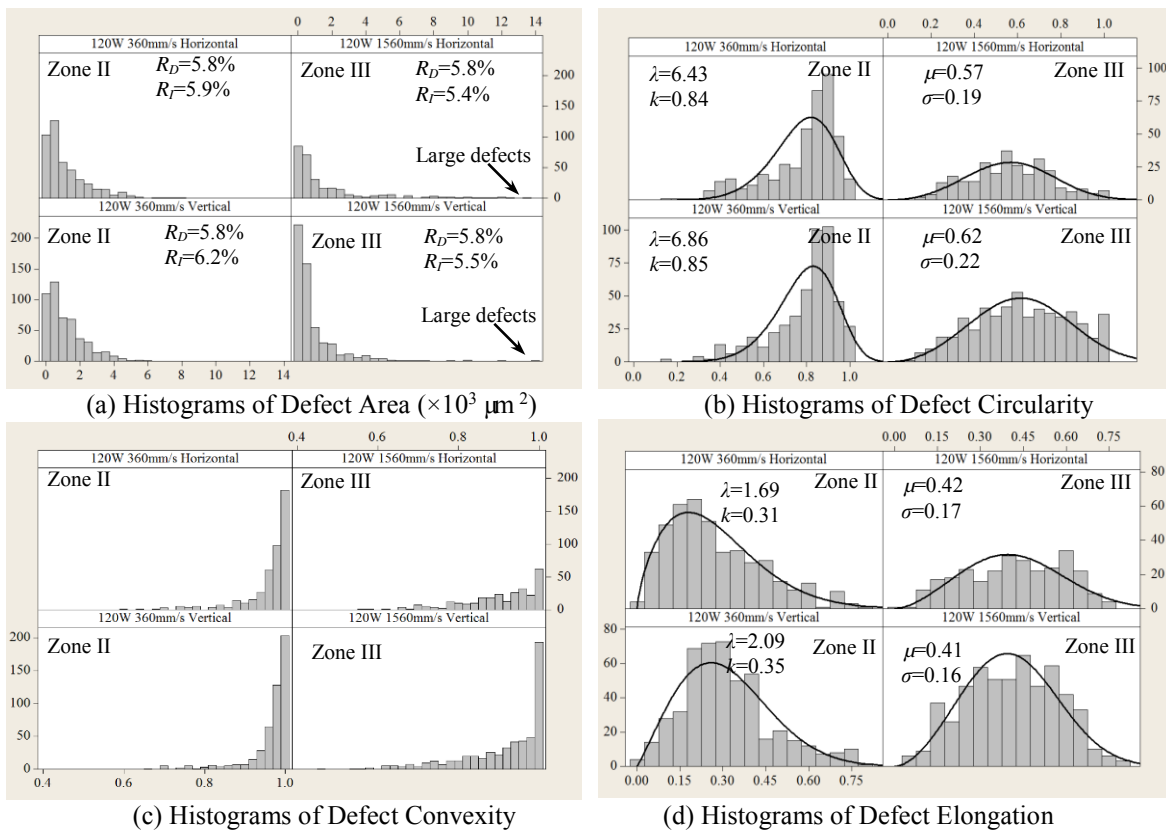


Fig. 10 Distribution of Defect Morphology of SLM-produced Zone II and III (Porosity \approx 5.8%)

Zone III defects are formed between melt pools or hatch lines due to insufficient energy density. Thus, it makes sense that Zone III defects are spread stochastically with irregular shape. Both circularity and elongation histograms of defects are normally distributed. An SLM Ti-6Al-4V top surface fabricated with marginal parameters is shown in Fig. 11.

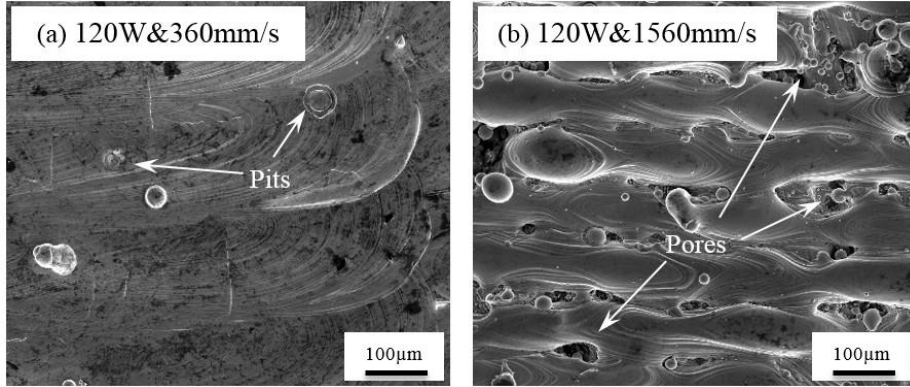


Fig. 11 Top Surfaces of SLM Specimens by Marginal Parameters (a) Zone II and (b) Zone III

When Ti-6Al-4V powder was melted using Zone II marginal parameters, the melt pool was extremely enlarged. Large melt pool results in a large overlap between hatch lines. However, no voids or defects were directly formed by the large melt pool and highly overlapped hatch lines. Spherical pits, as shown in Fig. 11 (a), are believed to cause spherical defects in Zone II specimens. These pits result from the recoating blade scraping particles, which are solidified from the ejected molten materials on the surface. This phenomenon is dramatic because Zone II marginal parameters melt the powder with high energy density. By contrast, the Zone III voids or pores directly generated on the top surface, as shown in Fig. 11 (b), are entrapped by new recoated and melted layers.

3.2 Characterization of EBM Defects

EBM defects resulted from the increased line offset and focus offset values. Energy density is decreased due to these marginal parameters. Compared to laser melting, EBM defects are formed similarly to Zone III defects in SLM. In this section, the morphology of line offset defects and focus offset defects are analyzed.

3.2.1 Defect Morphology of Line Offset (LO) Defects

Porosity dramatically increases when the line offset value is larger than 0.18mm, according to the porosity distribution curve in Fig. 2. Thus, Fig. 12 shows the cross sections of specimens at specific line offsets of 0.18mm, 0.22mm, 0.26mm, and 0.30mm.

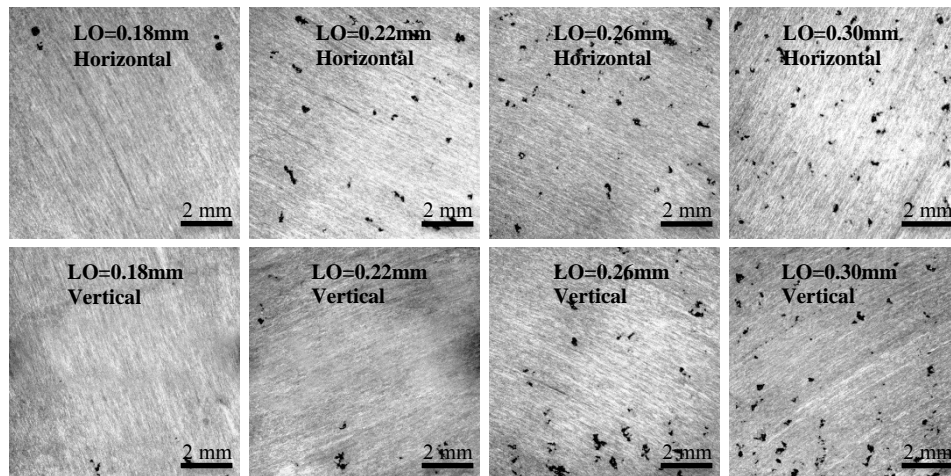
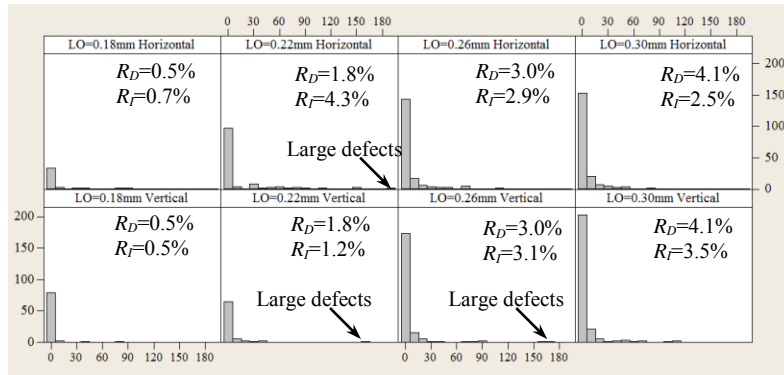
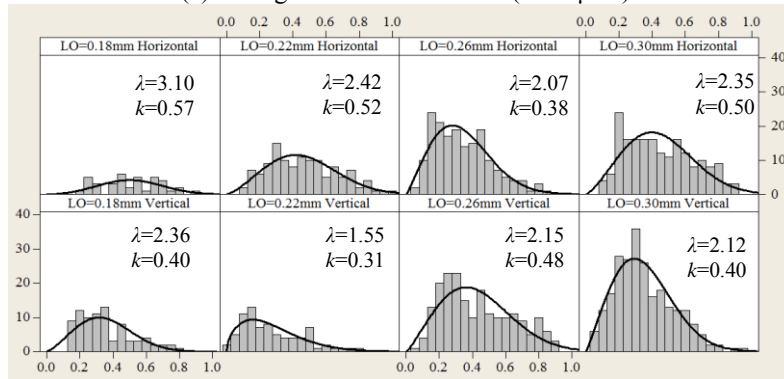


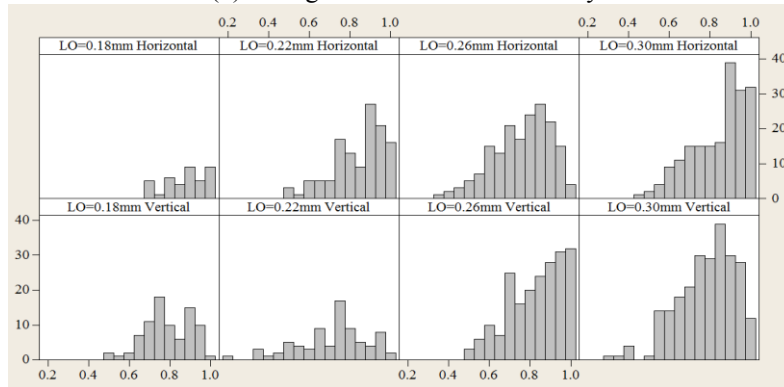
Fig. 12 Cross Sections of EBM-produced Specimen at Various Line Offset Values



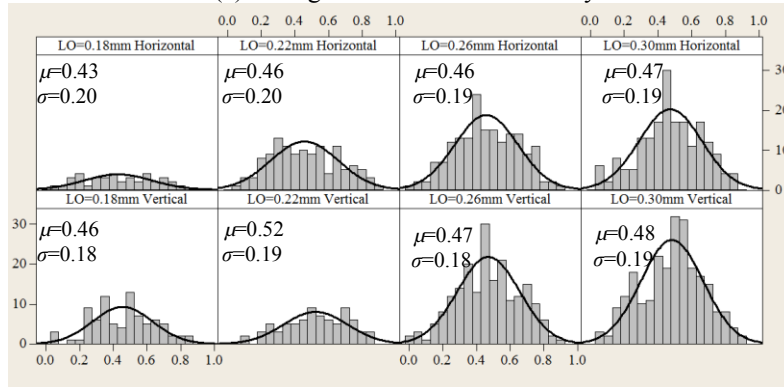
(a) Histograms of Defect Area ($\times 10^3 \mu\text{m}^2$)



(b) Histograms of Defect Circularity



(c) Histograms of Defect Convexity



(d) Histograms of Defect Elongation

Fig. 13 Distributions of Line Offset Defect Morphology of EBM-produced Specimens

LO defects are spread on the cross sections of Ti-6Al-4V specimens unequally. Large defects can be observed directly with bare eyes. It can be seen that, when line offset is 0.18mm there are only a few defects showing on the cross sections. However, as line offset increases, the defect amount increases correspondingly. As shown in Fig. 13 (a), most LO defect areas are smaller than $30 \times 10^3 \mu\text{m}^2$. Large defects are rare, but can have extremely large area. A Weibull fitting curve can be used to describe the distribution of the histograms of LO defect circularity. But the curve characteristics are very different from that of SLM Zone II or Zone III defects. From Fig. 13 (b), it is noted that all the fitting curves show left skewness, which means no defects have a circular contour. Thus, most EBM defects are very irregular.

Defect convexity, shown in Fig. 13 (c), verifies the irregularity of LO defects. Although many defects have a convexity value close to 1, there are a large amount of defects with small convexity values. This indicates that these defects have concave contour, as shown on the cross sections. Elongation of LO defects can be described by normal distribution fitting curves. All fitting curves, as shown in Fig. 13 (d), have mean values close to 0.50, and standard deviation close to 0.20. This is similar to Zone III defects of SLM specimens. Most LO defects (about 84%) have an elongation value less than 0.7.

3.2.2 Defect Morphology of Focus Offset (FO) Defects

Cross sections of Ti-6Al-4V specimens with FO defects are shown in Fig. 14. Large defects can also be observed with the naked eye from sectioned surface. Some defects are successive on the vertical cross sections. These defects are spread vertically from the bottom to the top surface. It is believed that an increased focus offset value generates an extended melt pool. But the reduced melting depth creates an unstable melt pool due to the underneath un-melted powder. Voids and pores are generated due to the instability of the melt pool. This means that FO defects are often created above the voids or pores of a previous layer. Thus, successive defects grows as shown in the vertical cross sections.

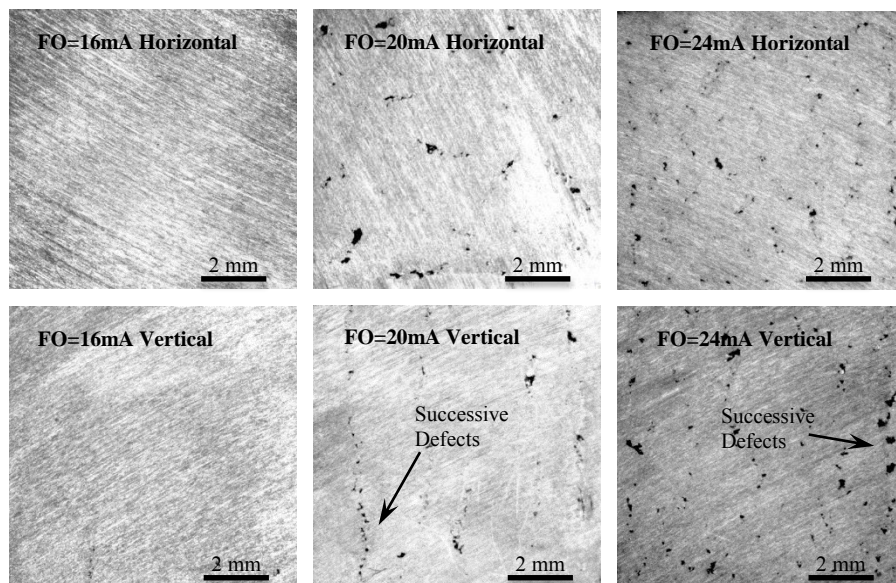


Fig. 14 Cross Sections of EBM-produced Specimen at Various Focus Offset Values

As for the morphology of FO defects, it can be seen, in Fig. 15 (a), that most defects are small, with an area less than $15 \times 10^3 \mu\text{m}^2$. Only a few large defects were found. The circularity

distribution of FO defects can also be described by Weibull fitting curves, as shown in Fig. 15 (b). Few defects show circular contour according to the left skewness of the distribution characteristics. Fig. 15 (c) shows the convexity of FO defects. Most defects have a concave contour. It is predictable that narrow and long defects exists in the specimens. A normal distribution can be used to describe the elongation of FO defects. Its statistical characteristics are similar to that of LO defects.

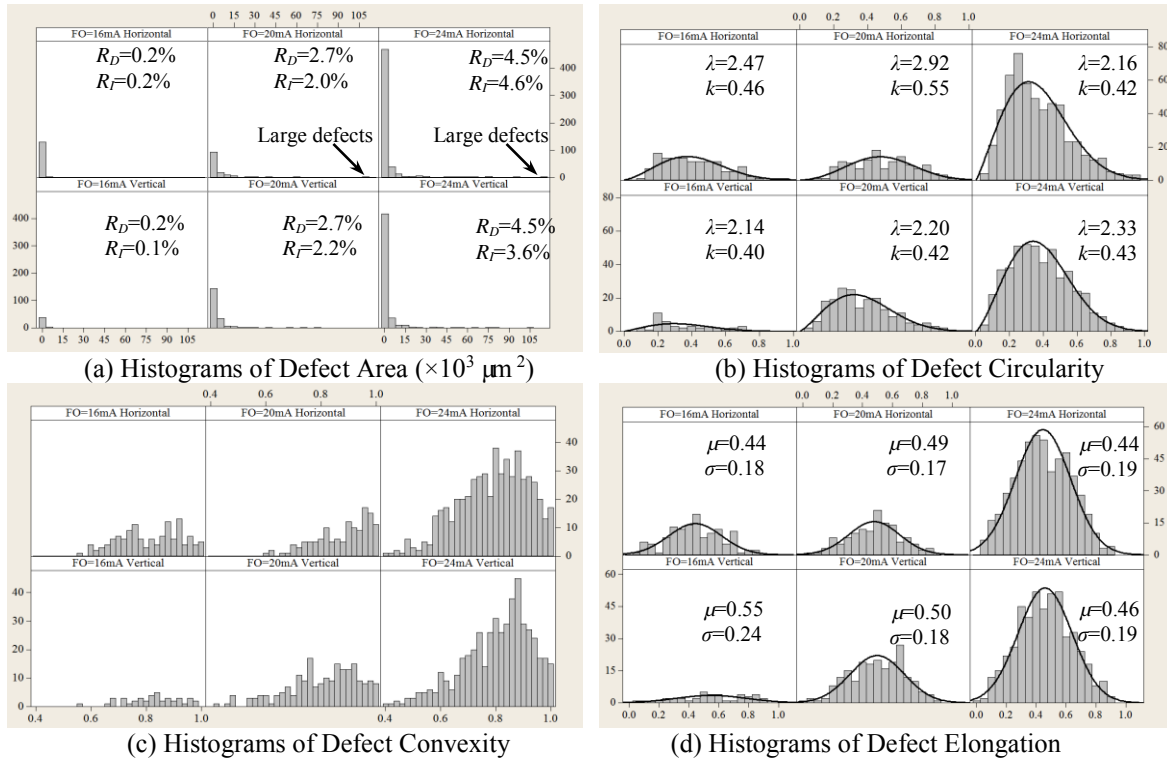


Fig. 15 Distribution of Focus Offset Defect Morphology of EBM-produced Specimens

3.2.3 Comparison between LO Defects and FO Defects

The morphological characteristics of LO defects and FO defects are similar, based on the defect area, circularity, convexity, and elongation distribution of histograms. Thus, it can be determined that the morphology of LO defects and FO defects are the same. The only difference is the spreading characteristics of defects in the specimens. From the cross section of EBM specimens, it can be seen that LO defects are randomly spread on the horizontal and vertical planes. It is hard to say any of defects are correlated with each other. However, successive FO defects are aligned in the vertical plane. The defects resulting from an increased focus offset more easily lead to the growing of defective region.

The formation of EBM defects can be further explained by the melt pool characteristics on the top surface. The melt pools are isolated from each other due to the increased line offset. Molten powder is easily fused together causing voids, as shown in Fig. 16 (a). Although melt pools are highly overlapped when increasing focus offset, a certain amount of powder underneath is not melted due to the shallow depth of the melt pools. The un-melted powder has an impact on the upper surface where voids are formed, as shown in Fig. 16 (b).

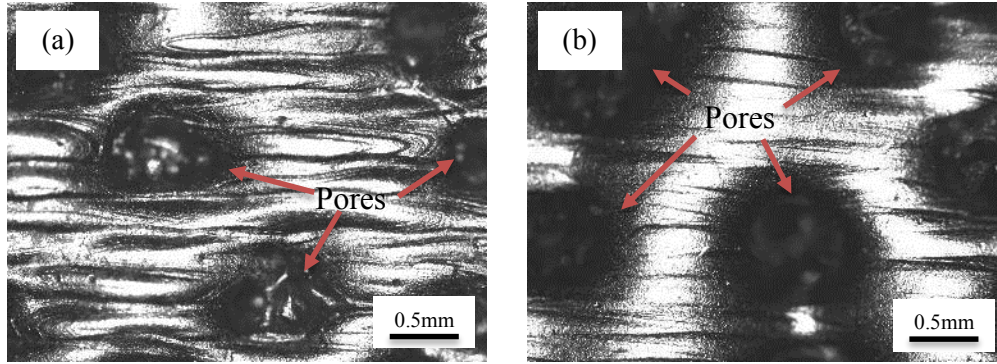


Fig. 16 Top Surface of EBM Specimens (a) LO=0.26mm and (b) FO=20mA

3.3 Image Processing Porosity R_I

The porosity R_D is obtained by measuring the specimen's relative density. It is considered an accurate method for estimating the porosity of SLM and EBM materials. R_I is used as a reference for estimating a specimen's porosity according to the ratio of defective area to the overall area of each cross section. It is notable that R_I is very close to R_D . It can be inferred that, if enough cross sections are processed, the image processing porosity R_I should be a feasible way of estimating the actual porosity of specimens. Although R_I has to be obtained from destructive characterization techniques, it enables the avoidance of lacquering or oil impregnation, which must be applied to the surface of porous parts to avoid penetration of fluid when using Archimedes method. Thus, image processing porosity can be considered an alternative way of estimating porosity of additively manufactured specimens.

4. Conclusion

Defect morphology of SLM and EBM specimens were studied using image processing to investigate defect area, porosity and other morphological characteristics such as circularity, convexity, and elongation. It can be concluded that higher porosity is usually accompanied with larger defect dimensions in both SLM and EBM specimens. Defect morphology can be correlated with melt pool characteristics.

Zone II defects formed by high energy density are distributed in SLM specimens and have a spherical shape. Porosity is a result of mechanically scraping the solidified particles, which are ejected from melt pool. A Weibull distribution can be used to describe the circularity and elongation of Zone II defects. Zone III defects, which are formed by low energy density levels, are irregular in shape in SLM. Defects are directly generated due to the insufficient energy for complete melting. Porosity is entrapped when new recoated and melted layers are applied over top. Circularity and elongation of Zone III defects are normally distributed.

Line offset defects and focus offset defects in EBM are all formed due to a reduced energy density, similarly to Zone III defects in SLM. Their irregularity can be attributed to the large pores formed on the top surface. There are nearly no circular defects in EBM specimens according to the circularity distribution. A certain amount of defects show concave characteristics.

Image processing porosity R_I can reflect the approximate porosity of porous parts. Thus, image processing can be a feasible way of estimating porosity if cross section images are well processed.

Acknowledgements

The authors gratefully acknowledge the support of the Office of Naval Research, awards N00014-09-1-0147 and N00014-10-1-0800, Technical Monitor: Dr. Ignacio Perez. The authors also express their gratitude to the staff of the Rapid Prototyping Center at the University of Louisville for their assistance.

Reference

- [1] I. Gibson, D.W. Rosen, B. Stucker. Additive Manufacturing Technologies: Rapid Prototyping to Direct Digital Manufacturing. Springer, New York, NY, 2009
- [2] L. Thijs, F. Verhaeghe, T. Craeghs, et al. A study of the microstructural evolution during selective laser melting of Ti-6Al-4V. *Acta Materialia*, 58(9), 2010, 3303-3312
- [3] M. F. Zaïh, S. Lutzmann. Modelling and simulation of electron beam melting. *Prod. Eng. Res. Devel.* 4(1), 2010, 15-23
- [4] W.O. Soboyejo, T.S. Srivatsan. Advanced Structural Materials: Properties, Design Optimization, and Applications. *CRC Press 2006*, 359-400
- [5] F.H. Sam Froes. Titanium Powder Metallurgy: A Review-Part 2. *Advanced Materials & Processes*, 170(10), 2012, 26-29
- [6] J. Schwerdtfeger, R. F. Singer, C. Koerner. In situ flaw detection by IR-imaging during electron beam melting. *Rapid Prototyping Journal*, 18(4), 2012, 259-263